ELSEVIER

Journal of Non-Crystalline Solids 239 (1998) 162–169

JOURNAL OF NON-CRYSTALLINE SOLIDS

Local structure of Er^{3+} in multicomponent glasses

P.M. Peters [1], S.N. Houde-Walter *

The Institute of Optics, College of Engineering and Applied Science, University of Rochester, Rochester, NY 14627-0186, USA

Abstract

Erbium environments in several multicomponent glasses are investigated using X-ray absorption fine structure spectroscopy on the Er L_{III}-edge. Glass hosts studied include aluminosilicate, fluorosilicate, phosphosilicate, alkali phosphate, fluoride, and another multicomponent silicate glass. The Er–O separation is found to vary only slightly between 2.21 and 2.25 Å. The first shell coordination number is dependent on glass host ranging from 6.3 nearest neighbor anions in the aluminosilicate glass to 10.0 in the fluoride host. The Debye–Waller factor for the first shell is also host dependent. It ranges from 0.021Å^2 in the phosphate hosts to 0.033 Å^2 in the aluminosilicate glass. While Er–Er correlations are observed in the crystalline Er_2O_3 standard, no evidence of molecular or short-range clustering of Er^{3+} ions is found in the glasses. Photoluminescence spectra are also presented for each of the glass hosts examined.

PACS: 61.10.Ht; 42.70.Hj; 61.43.Fs

1. Introduction

There has been a great deal of recent interest in miniature, rare earth doped glass devices. Both microchip lasers [1] as well as channel waveguide lasers, lossless splitters, [2] and amplifiers [3] have been demonstrated. Waveguide lasers are particularly interesting because of the freedom in cavity design as well as the potential for integrated optical components. Examples include dual output lasers [4], lasers emitting at multiple wavelengths [5] and Q-switched lasers [6].

Making a useful device which is only a few centimeters in length requires a large gain per unit length compared with fiber amplifiers which may be several meters long. Achievable gains are limited by the onset of concentration quenching at relatively low densities of rare earth ions (typically a fraction of a mol% depending on host glass). Fig. 1 shows energy level diagrams for the two processes which lead to concentration quenching in Er^{3+} doped glasses. Cooperative upconversion, or more correctly, summation of photon energies through energy transfer [7], is a process which directly results in the loss of an excited ion. The process occurs when two neighboring ions are in the $^4I_{13/2}$ excited state. The energy from one of the ions is transferred to the other leaving an ion in the $^4I_{15/2}$ excited state and the other in $^4I_{9/2}$ state.

Hydroxyl (OH) impurities in glass are also efficient quenchers. OH vibrational frequencies typically occur in the range 2.77–3.57 μm, which is higher than other vibrational frequencies in the glass [8]. As a result, only two or three phonons are usually required for nonradiative deexcitation of most rare earth in glass laser transitions. In addition, it is also possible for energy to migrate from

* Corresponding author. Tel.: +1-716 275 7629; fax: +1-716 271 1027; e-mail: shw@optics.rochester.edu.

[1] Also with USAF Wright-Patterson AFB, OH 45433, USA.

0022-3093/98/$ – see front matter
PII: S0022-3093(98)00733-9

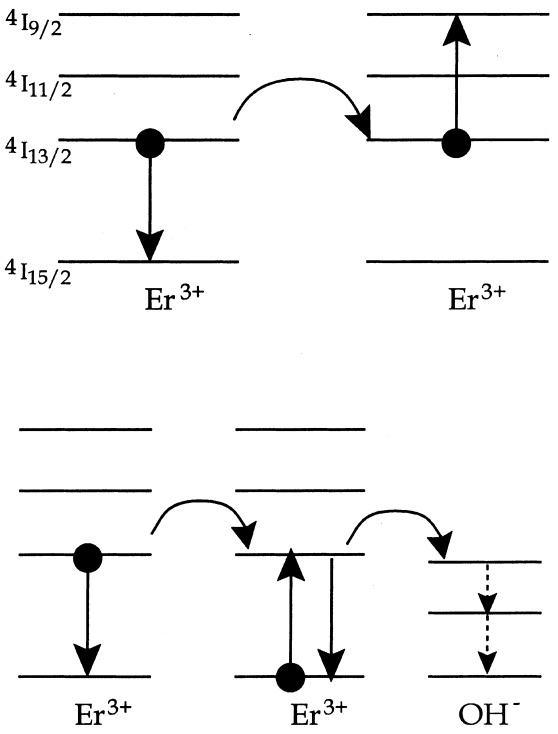

Fig. 1. Energy level diagrams showing known quenching processes for Er^{3+}. The top figure shows energy upconversion between two excited ions, while the bottom diagram depicts energy migration from excited Er^{3+} to non-excited Er^{3+} followed by quenching at OH.

an excited ion to a nonexcited ion via a resonant dipole–dipole interaction [9,10]. The probability of this energy transfer process is proportional to R^{-6}, where R is the distance between neighboring ions [11]. Experimental results, in which luminescent decay rates have been shown to increase with rare earth content, have been attributed to the process of energy migration followed by quenching at an OH [9,10,12]. Energy migration and subsequent quenching by OH is schematically illustrated in Fig. 1.

It has been commonly accepted that rare earth ions tend to cluster together at higher concentrations [13]. Clustering was first predicted for the Nd:SiO_2 system by Arai who also observed that the addition of codopants such as Al and P tended to reduce concentration quenching, and should therefore help to break up clusters [14]. Pure silica is nominally made up of SiO_4 tetrahedra with all bridging oxygen. Rare earth ions with larger ionic radii which are typically 6+ coordinated are not easily incorporated into the rigid network of vitreous silica.

Now, a variety of multicomponent glasses are used as hosts for Er^{3+}. The environment of the rare earth ion obviously plays an important role in determining the optical properties of the glass host being considered. Several studies of rare earth environments in glass have been reported recently including X-ray absorption fine structure (XAFS) studies of various rare earths in silicate [15], metaphosphate [16], borate [17], and fluorozirconate [18,19] glasses. A recent nuclear magnetic resonance study of neodymium doped silica is the only examination of rare earth doped glasses to report direct structural evidence of clustering [20].

XAFS is a powerful tool for obtaining information about the environments of constituents in multicomponent systems such as glass which do not possess long range order. A subset of the results reported here were reported in an earlier paper [21]. In that paper we established that the environment of Er^{3+} was not dependent upon the concentration of Er^{3+} and that there was no evidence of clustering at XAFS detectable distances in the three glass hosts being considered. In this paper we expand the number of glass hosts being considered to include many of the materials currently being used to build waveguide laser devices. Photoluminescence measurements are also included.

2. Experimental

2.1. Samples

XAFS data was collected on an Er_2O_3 crystalline standard and several glass compositions. Host glasses included batch-melt alkali phosphate, aluminosilicate, fluorosilicate, phosphosilicate, fluoride, and a multicomponent (commercial) silicate glass. Table 1 contains Er^{3+} contents of the samples which were investigated along with compositional information when available. In addition, a sample of the Schott multicomponent glass was co-coped with 2 mol% Yb_2O_3 and 1 mol% Er_2O_3.

Table 1
Glass Er^{3+} contents and available compositions

Glass name	Glass type	Composition (mol%)
AS	Aluminosilicate	59 SiO_2, 20 Na_2O, 20 Al_2O_3, 1 Er_2O_3
MS1	Silicate	multicomponent–2.5 Er_2O_3
MS2	Silicate	multicomponent–2 Yb_2O_3, 1 Er_2O_3
FS1	Fluorosilicate	1.7 Er_2O_3
FS2	Fluorosilicate	0.4 Er_2O_3
AP	Alkaliphosphate	58 P_2O_5, 13 Al_2O_3, 23 Na_2O, 6 Er_2O_3
PS	Phosphosilicate	50 P_2O_5, 30 SiO_2, 17 Na_2O, 3 Er_2O_3
F	Fluoride	36.5 AlF_3, 9.5 YF_3, 20 CaF_2, 10 BaF_2, 10 MgF_2,10 SrF_2, 4 ErF_3

2.2. XAFS

Er L_{III}-edge (8358 eV) X-ray absorption spectra were acquired at the Cornell High Energy Synchrotron Source (CHESS) [22] on stations B-2 and F-2. The transmission method was utilized for all samples. The reference and sample detectors consisted of 10 cm long nitrogen filled ion chambers. A Si (1 1 1) double-crystal monochromator with 50% harmonic rejection was used. The data range extended from 200 to 500 eV above the absorption edge, with a post-edge energy step of 3 eV. Multiple scans were averaged together with a total acquisition time of approximately 1–5 h per sample. The glasses were powdered and then mounted on Scotch tape. Multiple layers were stacked to obtain an absorption-thickness product of approximately 2.

XAFS data analysis was performed using the package developed by the Daresbury Synchrotron Laboratory. EXBACK was used to remove the fine structure from the raw absorption spectra by fitting low (2nd or 3rd) order polynomials to the post absorption edge region. EXCURV88 [23] was used to compare the XAFS data to the curved wave theory of XAFS [24]. The structural parameters included in the curved wave theory are the coordination number, N, the radial distance, r, and the Debye–Waller factor, $2\sigma^2$.

Data was also acquired on the crystalline standard Er_2O_3. In analyzing the crystal data, the structural parameters are constrained by the crystal structure as known from X-ray diffraction (XRD) studies. The non-structural XAFS fitting parameters (fraction of electrons participating in the XAFS process and the shake-off factor [21] are then varied until a good agreement is reached between the Er environment as determined by XAFS and by XRD. When such agreement is reached, the non-structural parameters are then fixed in the glass analysis, and are then considered transferable to the glass environment. Both the experimental and theoretical k^3-χ and partial radial distribution functions for Er_2O_3 are shown in

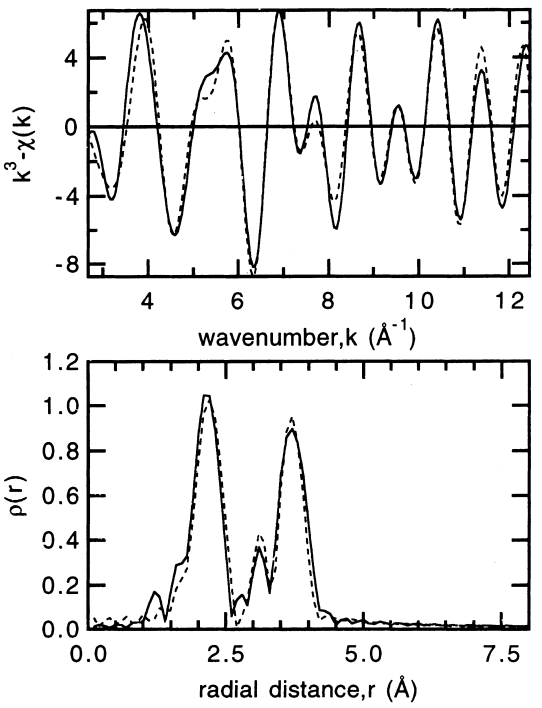

Fig. 2. k^3-weighted Er L_{III} XAFS (top) and partial radial distribution function (bottom) of Er_2O_3. Both experimental data (solid) and a theoretical curve fit (dashed) are shown. See Table 2 for structural determinations.

Table 2
Environment of Er in Er_2O_3 determined by XAFS and X-ray diffraction (See reference 23)

XAFS environment			crystallographic environment	
Corrd. no. N	Shell radius r (Å)	Debye–Waller factor $2\sigma^2$ (Å^2)	Coord. no. N	Shell radius r (Å) (average of 2 sites)
6 O	2.26	0.016	6 O	2.272
6 Er	3.49	0.014	6 Er	3.501
6 Er	3.98	0.093	6 Er	3.991

Fig. 2. Table 2 gives a comparison of the environment of Er in this crystal as determined by XAFS and XRD [25].

2.3. Photoluminescence

The photoluminescence from the $^4I_{13/2}$ level of Er^{3+} was measured by exciting the samples with the 514.5 nm line from an Ar^+ ion laser. Approximately 200 mW was incident on polished glass samples in an unfocused ~3 mm spot size. The fluorescence was focused onto the slits of a 0.35 m double grating monochromator and collected with a liquid nitrogen cooled Ge detector. The resolution of the monochromator was 6 Å/100 μm slit width. The slit width that was used varied from 80 to 350 μm depending on the fluorescence signal level from the sample. All optical measurements were performed at room temperature.

3. Results

3.1. XAFS

Often constituents of oxide glasses are found to take on a short range environment which is similar to their crystalline oxide counterpart. XAFS measurements on Er_2O_3 clearly reveal the Er shell at 3.5 Å, as well as a more distant Er shell at 3.99 Å (see Table 2). We expect then, that if clusters of Er^{3+} ions were present in heavily doped glasses that the Er–Er separation in these clusters would likely be in the XAFS detectable range of ~4 Å.

Fig. 3 shows XAFS and a Fourier transform partial radial distribution function for a phosphosilicate glass (PS) which contains 3 mol% Er_2O_3. Experimental data and a theoretical curve fit are included, along with a transform of both. Table 3 gives the first shell fit parameters for all glasses under study. Typical errors for XAFS analysis of first shell glass environments are $\Delta N = \pm 0.5$ atom, $\Delta r = \pm 0.02$ Å, and $\Delta 2\sigma^2 = \pm 0.005$ Å. Fig. 4 contains the experimental partial radial distribution functions for all glass hosts examined in order to allow a qualitative comparison of the XAFS data.

For most cases, two or even three shells could be resolved from the XAFS data. The XAFS could

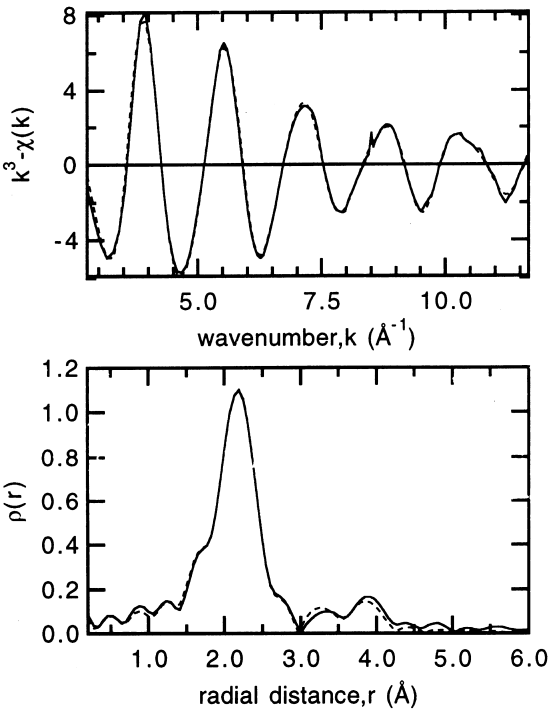

Fig. 3. k^3-weighted Er L_{III} XAFS (top) and partial radial distribution function (bottom) of phosphosilicate glass (PS) doped with 3 mol% Er_2O_3. Both experimental data (solid) and a theoretical curve fit (dashed) are shown. See Table 3 for structural determinations.

Table 3
First Shell Er environment determined by XAFS

Host Glass	First shell			Second shell radius (Å)	Third shell radius (Å)
	Coord. number (N)	Shell radius r (Å)	Debye–Waller factor $2\sigma^2$ (Å^2)		
Er_2O_3	6.0 O	2.26	0.016	3.49	3.98
AS	6.3 O	2.21	0.033	3.55	3.79
MS1	6.6 O	2.22	0.023	3.52	3.79
MS2	6.8 O	2.22	0.025	3.53	3.80
FS1	7.5 O/F	2.23	0.031	3.57	3.82
AP	7.2 O	2.23	0.021	3.52	3.78
PS	7.5 O	2.25	0.021	3.55	3.78
F	10.0 F	2.22	0.029	3.68	–

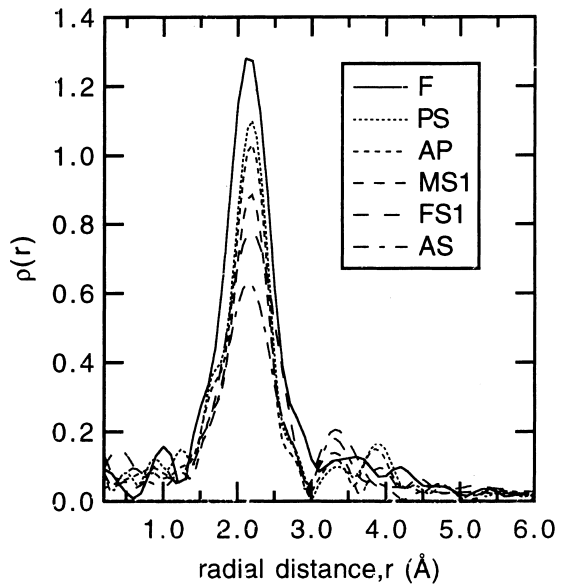

Fig. 4. Superposition of experimental partial radial distribution functions of all glasses. See Table 1 for a description of the different glasses and Table 3 for structural determinations.

accurately determine the radii of these distant coordination shells, and these are also included in Table 3. However, the coordination number and disorder could not be accurately determined for the distant second and third coordination shells. The data was most consistent with a light element such as Si, P, or Al being found in these shells. Placing a heavier ion, such as Er in these shells leads to a reduction in the quality of fit index.

Fig. 5 shows room temperature photoluminescence spectra for the different glass hosts under consideration. Table 4 gives the peak fluorescence wavelength along with the effective linewidth,

$$\Delta\lambda_{\text{eff}} = \frac{\int I(\lambda)\,\mathrm{d}\lambda}{I_{\text{peak}}}, \tag{1}$$

for each sample.

4. Discussion

It is evident from an examination of the XAFS results that the Er^{3+} local environment varies with glass host composition. However, in XAFS data analysis, it must be noted that the coordination number, N, and the Debye–Waller factor, $2\sigma^2$, are correlated parameters. It is possible to increase or decrease both simultaneously, over some range, without a change in the quality of fit. Therefore, to investigate whether differences in coordination number and disorder factor are statistically significant, it is useful to plot correlation maps for the two parameters (see Fig. 6). The maps are created by varying N and $2\sigma^2$ around the magnitudes which are found to minimize the least-squares fit index. The ovals correspond to a maximum change in the fit index of 5%. If the environments in the various glass hosts are distinct, the contours for different glass types are separated from each other. Fig. 6 shows clearly that Er^{3+} has a different local environment in the various hosts.

Er^{3+} in the aluminosilicate (AS) sample has an environment which is somewhat similar to the crystalline Er_2O_3 environment. The first coordination shell in the sample consists of an average of

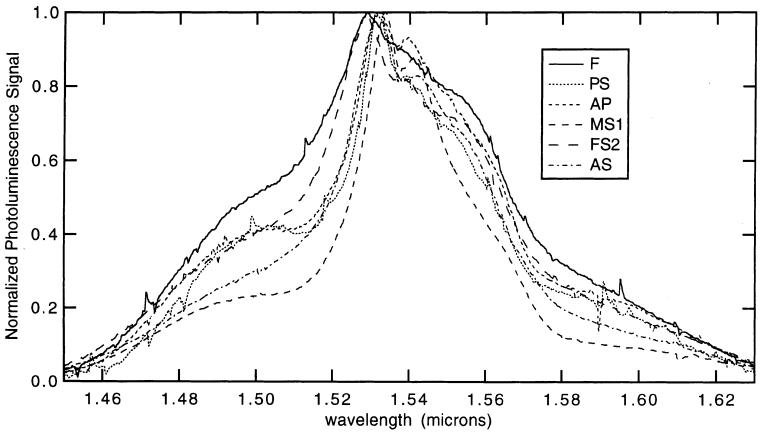

Fig. 5. Photoluminescence spectra of all Er^{3+} glasses studied excited by 514.5 nm light. See Table 4 for peak wavelengths and linewidths.

Table 4
Photoluminescence data

Host glass	Peak λ (nm)	$\Delta\lambda_{eff}$ (nm)
AS	1532	59.3
MS	1534	49.3
FS2	1529	69.1
AP	1532	67.9
PS	1531	61.2
F	1529	77.4

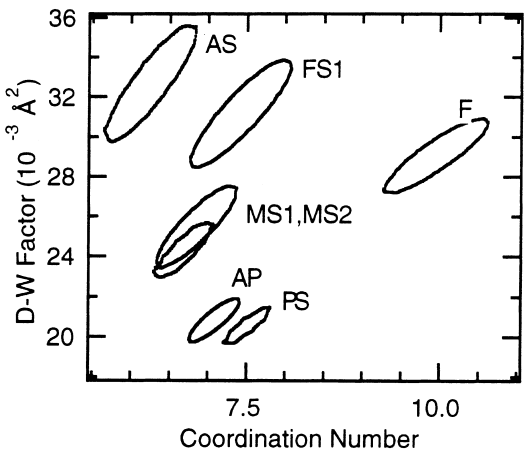

Fig. 6. Correlation map of coordination number and Debye–Waller factor for Er^{3+} doped glasses. Nonoverlapping contours indicates distinct Er^{3+} environments.

6.3 oxygen at a radial distance of 2.21 Å, while in Er_2O_3, Er is surrounded by 6 O at a distance of 2.263 Å. The disorder factor is larger in the sample than in the crystal sample (see Table 3), as expected. In the fluoride sample (F) the coordination number is larger than in any of the oxide based glass hosts. The fluoride sample we examined had an average coordination number of 10.0 F at a radial distance of 2.221 Å. By comparison, Er in ErF_3 has 9 nearest neighbor F at an average distance of 2.31 Å. The fluorosilicate mixed anion sample (FS1) has a coordination number of 7.5 which is intermediate to the endpoint single anion hosts.

The alkali phosphate (AP) and phosphosilicate (PS) samples have similar, although still distinct environments. The coordination number is larger than in the simple aluminosilicate sample (AS) at 7.2 to 7.5 oxygen anions. The first shell Debye–Waller disorder factors are smaller than those of any of the other samples studied (see Table 3). It is known that more rare earth ions can be incorporated into a phosphate host glass than in other common glasses, before the onset of concentration quenching [26]. Phosphate glasses which contain sufficient alkali metal are made up of long chains of PO_4 units which contain only two bridging oxygen [27]. Therefore, when the rare earth is introduced into the phosphate glass it is able to deform the phosphate chain network about itself

forming a well ordered, and perhaps more isolated environment.

It is also noteworthy that the Er^{3+} environment in the phosphate samples apparently less sensitive to changes in the glass composition than the silicate samples. Note that in the 3 samples in which Si is the network former, changes in glass composition lead to larger changes in Er^{3+} local environment. Conversely, adding 30 mol% SiO_2 to the alkali phosphate composition causes a much smaller change in the environment of the rare earth dopant ions. It is not likely a coincidence that in the multicomponent silicate laser sample (MS1,MS2) the Er^{3+} first shell coordination number increases and Debye–Waller factor decreases such that the environment in this glass is more similar to a phosphate sample than any of the other silicate samples. This laser glass sample has been optimized to produce the best laser glass possible given the other constraints such as desirable mechanical properties and refractive index requirements.

Table 3 also indicates that the Er^{3+} environments in the two multicomponent silicate samples are identical. One of these is doped only with Er_2O_3 (MS1) while the other is doped with both Er_2O_3 and Yb_2O_3 (MS2). This identity indicates the absence of Er–Yb molecular clusters and implies that the interaction between Yb^{3+} and Er^{3+} is a relatively long range interaction (several Å). Such co-doped glasses have been used to make waveguide laser devices which are pumped on the 960 nm $^2F_{7/2} \rightarrow {}^2F_{5/2}$ of Yb^{3+} and which lase on the $^4I_{13/2} \rightarrow {}^4I_{15/2}$ transition of Er^{3+} at 1550 nm [28].

The fact that no short-range clustering of Er^{3+} ions is evident in these glasses indicates that rare earth clustering is a problem which may be unique to SiO_2. The fact that clusters of rare earth ions do not exist in multicomponent glass systems was suggested earlier [26], although never proven. The consequence of the apparent lack of clustering is that the degradation of excited state lifetimes at high erbium concentrations (e.g. see data reported in Refs. [9,10,21]) is the result of the interaction of rare earth ions at long distances.

Photoluminescence is also a sensitive probe of the local environments of the active ions in a host glass. Since each rare earth ion sits in a unique site, the ligand field experienced by each ion differs [26]. This difference leads to different Stark levels for each ion. The greater the disorder in the rare earth environment, the greater the differences in Stark levels, leading to a photoluminescence spectrum over a larger range of wavelength and differences in the peak photoluminescence wavelength. There is a difference in peak wavelength of up to 5 nm among the six sample compositions studied. There is not a one to one correspondence between the Debye–Waller factor (Table 3) and the effective linewidth (Table 4), since there are other factors which affect spectral broadening. We can note, however, that two glasses with larger disorder, the fluorosilicate (FS) and the fluoride (F), have the broadest emission spectra, while the multicomponent silicate (MS) which has low disorder, has the narrowest spectrum of all.

5. Conclusions

XAFS studies of erbium doped aluminosilicate, fluorosilicate, multicomponent silicate, phosphosilicate, alkali phosphate, and fluoride samples indicate variations in the local environment of the active Er^{3+} ions as a function of composition. No evidence of short-range clustering of Er^{3+} ions is found, indicating that concentration quenching in heavily doped glasses is the result of long range interactions between active ions (over several Å). The variations in local environments determined by XAFS are corroborated by photoluminescence spectra. The effective linewidths of the glasses studied vary from 49.3 to 77.4 nm.

Acknowledgements

Thanks are due to J. Dickinson of Corning, Inc., J. Hayden of Schott Glass Technologies and A. Kucuk and A. Clare of Alfred University for providing the samples which were used in this study. Thanks are also due to A. Bauco, D. Kominsky, K. Averrett, C. Hsieh, S. Poling, E. Ortiz and the staff at CHESS for assistance with XAFS measurements. P.M.P. is a participant in the US

Air Force Palace Knight Program. This research is supported by the NSF under Grant No. DMR-9612267.

References

[1] J.J. Zayhowski, Proceedings of the Conference on Lasers and Electro-Optics'97, paper CThK1.
[2] P. Camy, J.E. Roman, F.W. Willems, M. Hempstead, J.C. Van Der Plaats, C. Prel, A. Beguin, A.M.J. Koonen, J.S. Wilkinson, C. Lerminiaux, Electron. Lett. 32 (1996) 321.
[3] K. Hattori, T. Kitagawa, M. Oguma, M. Wada, J. Temmyo, M. Horiguchi, Electron. Lett. 29 (1993) 357.
[4] N.A. Sanford, K.J. Malone, D.R. Larson, R.K. Hickernell, Opt. Lett. 16 (1991) 1168.
[5] K.J. Malone, N.A. Sanford, J.S. Hayden, Electron. Lett. 29 (1993) 691.
[6] E.K. Mwarani, D.M. Murphy, M. Hempstead, L. Reekie, J.S. Wilkinson, Photon. Tech. Lett. 4 (1992) 235.
[7] F. Auzel, J. Lumin. 45 (1990) 341.
[8] E.G. Bondarenko, E.I. Galant, S.G. Lunter, A.K. Przhevulskii, M.N. Tolstoi, Sov. J. Opt. Technol. 42 (1975) 333.
[9] Y. Yan, A.J. Faber, H. de Waal, J. Non-Cryst. Solids 181 (1995) 283.
[10] E. Snoeks, P.G. Kik, A. Polman, Opt. Mater. 5 (1996) 159.
[11] D.L. Dexter, J.H. Schulman, J. Chem. Phys. 22 (1954) 1063.
[12] H. Ebendorff-Heidepriem, W. Seeber, D. Ehrt, J. Non-Cryst. Solids 183 (1995) 191.
[13] E. Desurvire, Erbium-Doped Fiber Amplifiers: Principles and Applications, Wiley, New York, 1994, p. 291.
[14] K. Arai, H. Namikawa, K. Kumata, T. Honda, I. Yoshiro, T. Handa, J. Appl. Phys. 59 (1986) 3430.
[15] M.A. Marcus, A. Polman, J. Non-Cryst. Solids 136 (1991) 260.
[16] D.T. Bowron, G.A. Saunders, R.J. Newport, B.D. Rainford, H.B. Senin, Phys. Rev. B 53 (1996) 5268.
[17] Y. Shimizugawa, N. Sawaguchi, K. Kawamura, K. Hirao, J. Appl. Phys. 81 (1997) 6657.
[18] W.-C. Wang, Y. Chen, T.-D. Hu, J. Appl. Phys. 79 (1996) 3477.
[19] P. Santa-Cruz, D. Morin, J. Dexpert-Ghys, A. Sadoc, F. Glas, F. Auzel, J. Non-Cryst. Solids 190 (1995) 238.
[20] S. Sen, J.F. Stebbins, J. Non-Cryst. Solids 188 (1995) 54.
[21] P.M. Peters, S.N. Houde-Walter Appl. Phys. Lett. 70 (1997) 541.
[22] Cornell High Energy Synchrotron Source, Cornell University, Ithaca, NY 14853.
[23] S.J. Gurman, N. Binsted, I. Ross, J. Phys. C 17 (1984) 143; S.J. Gurman, N. Binsted, I. Ross, J. Phys. C 19 (1986) 1845.
[24] P.A. Lee, J.B. Pendry, Phys. Rev. B 11 (1975) 2795.
[25] R.W.G. Wyckoff, Crystal Structures, vol. 2, Interscience, New York, 1964, pp. 4–5.
[26] W.J. Miniscalco, J. Lightwave Technol. 9 (1991) 234.
[27] S.W. Martin, Eur. J. Solid State Inorg. Chem. 28 (1991) 271.
[28] G.L. Vossler, C.J. Brooks, K.A. Winik, Electron. Lett. 31 (1995) 1162.